Acta Pharmaceutica Sinica B 2021;11(1):100–111

Chinese Pharmaceutical Association
Institute of Materia Medica, Chinese Academy of Medical Sciences

Acta Pharmaceutica Sinica B

www.elsevier.com/locate/apsb
www.sciencedirect.com

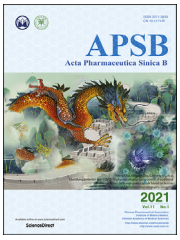

ORIGINAL ARTICLE

The antimicrobial peptide YD attenuates inflammation *via* miR-155 targeting CASP12 during liver fibrosis

Zhibin Yan[a], Dan Wang[a], Chunmei An[a], Hongjiao Xu[b], Qian Zhao[b], Ying Shi[b], Nazi Song[b], Bochuan Deng[a], Xiaomin Guo[a], Jing Rao[a], Lu Cheng[a], Bangzhi Zhang[a], Lingyun Mou[a], Wenle Yang[a], Xianxing Jiang[b,*], Junqiu Xie[a,*]

[a]*Key Laboratory of Preclinical Study for New Drugs of Gansu Province, School of Basic Medical Sciences & Research Unit of Peptide Science, Chinese Academy of Medical Sciences, 2019RU066, Lanzhou University, Lanzhou 730000, China*
[b]*School of Pharmaceutical Sciences, Sun Yat-sen University, Guangzhou 510006, China*

Received 20 May 2020; received in revised form 18 June 2020; accepted 7 July 2020

KEY WORDS

Liver fibrosis;
Inflammation;
Antimicrobial peptide;
MiR-155;
CASP12

Abstract The antimicrobial peptide APKGVQGPNG (named YD), a natural peptide originating from *Bacillus amyloliquefaciens* CBSYD1, exhibited excellent antibacterial and antioxidant properties *in vitro*. These characteristics are closely related to inflammatory responses which is the central trigger for liver fibrosis. However, the therapeutic effects of YD against hepatic fibrosis and the underlying mechanisms are rarely studied. In this study, we show that YD improved liver function and inhibited the progression of liver fibrosis by measuring the serum transaminase activity and the expression of α-smooth muscle actin and collagen I in carbon tetrachloride-induced mice. Then we found that YD inhibited the level of miR-155, which plays an important role in inflammation and liver fibrosis. Bioinformatics analysis and luciferase reporter assay indicate that *Casp12* is a new target of miR-155. We demonstrate that YD significantly decreases the contents of inflammatory cytokines and suppresses the NF-κB signaling pathway. Further studies show that transfection of the miR-155 mimic in RAW264.7 cells partially reversed the YD-mediated CASP12 upregulation, the downregulated levels of inflammatory cytokines, and the inactivation of the NF-κB pathways. Collectively, our study indicates that YD reduces inflammation through

*Corresponding authors. Tel.: +86 931 8915522; fax: +86 931 8911255.
E-mail addresses: jiangxx5@mail.sysu.edu.cn (Xianxing Jiang), xiejq@lzu.edu.cn (Junqiu Xie).

Peer review under responsibility of Chinese Pharmaceutical Association and Institute of Materia Medica, Chinese Academy of Medical Sciences.

https://doi.org/10.1016/j.apsb.2020.07.004

the miR-155−*Casp12*−NF-κB axis during liver fibrosis and provides a promising therapeutic candidate for hepatic fibrosis.

1. Introduction

Liver fibrosis is a pathological condition resulting from tissue injury and characterized by excessive accumulation of extracellular matrix (ECM)[1]. Common etiologies include chronic viral hepatitis, alcoholic liver disease, autoimmune disease, and nonalcoholic fatty liver disease/nonalcoholic steatohepatitis[2]. This condition is the common pathway of all kinds of progressive liver diseases leading to cirrhosis and even liver cancer, and regression at this stage is critical to prevent the progression of liver disease[3]. Inhibiting liver fibrosis, therefore, is a good approach to slow the progression of severe liver disease. However, there are no effective anti-fibrotic therapies to prevent the development of liver fibrosis, and the identification of satisfactory therapeutic agents for liver fibrosis is urgently needed.

MicroRNAs (miRNAs) are powerful post-transcriptional regulators that bind to the 3′ untranslated region (UTR), thus inhibiting complementary mRNA translation[4]. Accumulating evidence from animal experiments and clinical studies has shown that miRNAs have pivotal roles in the regulation of a variety of cellular activities in normal cell functions as well as in disease development, including inflammation, immunity, and infection[5]. MiR-155 was reported to be a vital regulator of inflammatory responses, and aberrant expression of this molecule has been detected in many different human diseases[6,7]. A recent report by Bala et al.[8] indicated that miR-155 was upregulated in the mouse model of alcoholic liver disease, whereas alcohol-induced inflammation and carbon tetrachloride (CCl_4)-induced liver fibrosis were attenuated in miR-155 knockout mice. Furthermore, miR-155 aggravated lipopolysaccharide (LPS)-induced inflammatory responses[9], while the inhibition of miR-155 ameliorated macrophage inflammation[10]. In addition, miR-155 has been intensively studied for the treatment of hepatic fibrosis because it targets several fibrogenesis genes[8,11,12].

The potent cationic glycine-rich antimicrobial peptide APKGVQGPNG (named YD, Fig. 1A), which was purified from *Bacillus amyloliquefaciens* CBSYD1, possessed activity against Gram-positive, Gram-negative, and multidrug-resistant (MDR) bacteria, and the mechanism involved cell-penetrating translocation inside the cells and interaction with DNA molecules[13]. In addition, another study from the same team revealed that YD had strong antioxidant potential *via* nuclear factor erythroid 2-related factor 2 (NRF2) mediated hemeoxygenase-1 expression[14]. The role of inflammation in the process of fibrosis prompted us to investigate the functional effect of YD during fibrosis. The objectives of the present study are mainly to evaluate whether treatment with YD would protect against CCl_4-induced experimental hepatic fibrosis, and to investigate the mechanisms underlying these beneficial properties. In this study, we demonstrate that YD could partially suppress inflammation by downregulating the miR-155 levels. Further studies confirmed that *Casp12* is a target of miR-155, and that the anti-fibrotic properties of YD are mediated through the miR-155−*Casp12*−NF-κB pathway. Our results show that YD may be developed as a promising compound for the treatment of liver fibrosis.

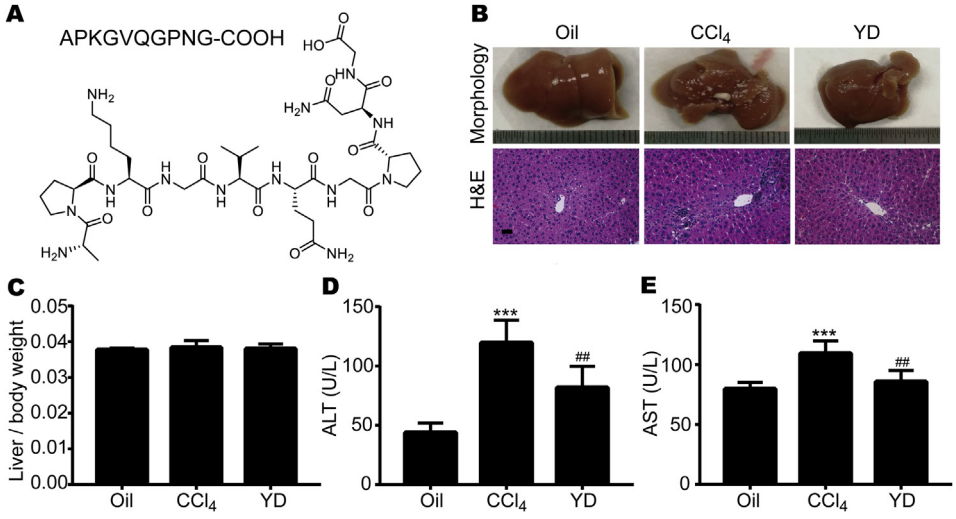

Figure 1 Effects of the antimicrobial peptide APKGVQGPNG (YD) on carbon tetrachloride (CCl_4)-induced liver injury. (A) Chemical structure of YD. (B) The representative photos of liver morphology and hematoxylin and eosin (H&E) staining (scale bar, 50 μm). (C) Effect of YD on the liver to body weight ratio in mice. (D) Serum alanine aminotransferase (ALT) activity. (E) Serum aspartate aminotransferase (AST) activity. Data are mean ± standard deviation (SD), $n = 6$. $^{***}P < 0.001$ *vs.* the oil group; $^{\#\#}P < 0.01$ *vs.* the CCl_4-induced group.

2. Materials and methods

2.1. Peptide synthesis

YD was synthesized on 2-chlorotrityl chloride resin (Energy Chemical, Shanghai, China) by the solid phase technique using *N*-9-fluorenylmethoxycarbonyl chemistry. The purity of the peptide was performed by reversed-phase high-performance liquid chromatography (RP-HPLC, Waters Corp., Milford, MA, USA), and the atomic accumulation of the peptide was verified using electrospray ionization mass spectrometry (ESI-MS, MaXis 4G, Bruker, Billerica, MA, USA).

2.2. Animals and experimental protocols

All animals received care in accordance with the Principles of Laboratory Animal Care formulated by the National Institutes of Health and the guidelines of the Laboratory Animals Use Committee of Sun Yat-sen University (Guangzhou, China). C57BL/6J mice (7-week-old males) were obtained from the Experimental Animal Center of Sun Yat-sen University and adapted to the laboratory conditions for 1 week before the experiments. The mice were kept in a room with a 12 h light/dark cycle, constant temperature, and humidity (25 $\pm$ 1 °C and 55 $\pm$ 5%, respectively). The animals had free access to food and clean water *ad libitum*.

The mouse model of liver fibrosis was established by intraperitoneally (i.p.) injecting the animals with CCl_4 (Aladdin, Shanghai, China) dissolved in corn oil (1:4, *v*/*v*) twice a week (5 mL/kg) for 6 weeks. The control mice were injected with corn oil (Aladdin) alone at the same volume and frequency. Animals were randomly assigned to three groups at the 4th week as follows ($n = 6$, each group): (i) control mice injected with phosphate buffer saline (PBS, Thermo Fisher Scientific, Waltham, MA, USA), (ii) PBS-treated CCl_4 mice, and (iii) YD (500 μg/kg)-treated CCl_4 mice, and the animals were also given daily ip administration of PBS or YD. All mice were sacrificed at week 7, and then, the blood and liver tissues were gathered. After the liver samples were rinsed with isotonic saline, all tissues were dissected and stored at −80 °C.

2.3. Biochemical analyses

Serum alanine aminotransferase (ALT) and aspartate aminotransferase (AST) activities were measured by appropriate assay kits (Nanjing Jiancheng Bioengineering Institute, Nanjing, China) according to the manufacturer's instructions.

2.4. Cytokine assays

The tumor necrosis factor-α (TNF-α) and interleukin 1β (IL-1β) levels in murine plasma samples were detected using an enzyme-linked immunosorbent assay (ELISA) kit (Cloud-Clone Corp., Wuhan, China) according to the manufacturer's instructions. Absorbance was measured at 450 nm using a microplate reader.

2.5. Histological analyses

Liver samples were fixed in 10% neutral-buffered formalin, embedded in paraffin, and then sliced into 4-μm sections. After deparaffinization, dehydration by a graded sequence of ethanol and rehydration, the liver sections were stained with hematoxylin-eosin (H&E) and Sirius red reagents (Sangon Biotech, Shanghai, China). Histological changes were observed in randomly chosen histological fields using a microscope (KOSTER UMC 800T, Guangzhou Koster Scientific Instrument Co., Ltd., Guangzhou, China), and quantitative analysis was performed with ImageJ software (National Institutes of Health, Bethesda, MD, USA).

2.6. Immunohistochemistry

Tissue sections, which were 4-μm thick formalin-fixed and embedded in paraffin, were prepared as follows. The samples were dewaxed in xylene and rehydrated in alcohol. Then, antigen was retrieved in citrate buffer (10 mmol/L citric acid, pH 6.0) and 3% hydrogen peroxide was used to block the sections at room temperature for 10 min. The antibody was diluted with 10% bovine serum albumin (BSA, Sangon Biotech) at a ratio of 1:200, and incubated overnight at 4 °C. The protein was detected using 3,3′-diaminobenzidine (DAB) staining (Thermo Fisher Scientific). The nucleus was stained by hematoxylin. Photographs were obtained using a microscope (Guangzhou Koster Scientific Instrument Co., Ltd.).

2.7. Cell culture

LX-2, RAW264.7 (murine macrophage cell line), and 293T cells were acquired from the Type Culture Collection of the Chinese Academy of Sciences (Shanghai, China). The cells were cultivated in Dulbecco's modified Eagle's medium (Gibco, Carlsbad, CA, USA) added with antibiotics (100 U/mL penicillin and 100 μg/mL streptomycin, Gibco) and 10% fetal bovine serum (FBS, BI, Beit HaEmek, Israel). The cells were grown in an incubator at 37 °C and containing 5% CO_2. When cell confluence reached 80%−90% confluence, the cells were digested using 0.25% trypsin-ethylenediaminetetraacetic acid (EDTA, Gibco), and then seeded at a density of 2×10^5 cells/well in 6-well plates. Cells were serum starved overnight before experimental manipulation. LX-2 cells were incubated with YD for 48 h. For induction of inflammation, RAW264.7 cells were stimulated with 1 μg/mL LPS (Merck, St. Louis, MO, USA) followed by the incubation with YD (50 and 100 μmol/L) for 48 h. The experiments were performed in triplicate with three independent cultures.

2.8. Cell viability assay

The effects of YD on cell viability were evaluated by cell counting kit-8 (CCK-8, YEASEN, Shanghai, China) assay. LX-2, LO2, or RAW264.7 cells were seeded in 96-well plates at a density of 1×10^4 cells per well with increasing concentrations of YD for 48 h. Then, CCK-8 (10 μL) was added to the each well and cultured for 2 h. The absorbance at 450 nm was measured using a microplate reader (Flex Station 3, Molecular Devices, Palo Alto, CA, USA).

2.9. Western blotting

The proteins were obtained from whole cell lysates using radioimmunoprecipitation assay buffer (RIPA) buffer (Beyotime, Shanghai, China) and 1 mmol/L freshly added phenylmethylsulfonyl fluoride (PMSF, Beyotime). Then, the concentration of protein was tested using the bicinchoninic acid (BCA) protein assay kit (Thermo Fisher Scientific). Thirty micrograms protein samples were directly separated by 10% sodium dodecyl sulfate-polyacrylamide gel electrophoresis (SDS-PAGE). Then, it was transferred to polyvinylidene difluoride membrane (PVDF,

Immobilon-P^{SQ} transfer membranes, Merck Millipore, Billika, Germany). The membranes were blocked with 5% (*w*/*v*) skim milk (Sangon Biotech) for 1 h, and then incubated with appropriate primary antibodies overnight at 4 °C, followed by the incubation with horseradish peroxidase-conjugated secondary antibodies (Zhongshanjinqiao, Beijing, China) suitable for each primary antibody (1:10,000) for 1 h at room temperature. The bands were detected using an electrochemiluminescence (ECL) detection system (Clarity Western ECL substrate, Bio-Rad, Hercules, CA, USA). Primary antibodies used were as follows: α-smooth muscle actin (α-SMA, 1:1000; Abcam, Cambridge, UK), collagen type I alpha 1 (Col1a1, 1:500; Boster, Wuhan, China), CASP12 (1:1000; Santa Cruz, Dallas, TX, USA), TNF-α (1:1000; Santa Cruz), phospho-I-kappa-B-kinase beta (p-IKKβ, 1:1000; Abcam), IKKβ (1:1000; Abcam, Cambridge, UK), phospho-I kappa B-alpha (p-IκBα, 1:1000; Abcam), IκBα (1:1000; Abcam), p-P65 and P65 (1:500; Boster), histone-H3 (1:1000; Santa Cruz), and glyceraldehyde 3-phosphate dehydrogenase (GAPDH, 1:1000; Boster). The band intensities were calculated using Tanon-Image Software (Shanghai, China) and standardized to GAPDH, and the levels of phosphorylated proteins were shown as the ratios to the total proteins.

2.10. *Nucleocytoplasmic fractionation*

Nucleocytoplasmic fractionation was performed using an extraction kit for nuclear and cytoplasmic proteins (Bestbio, Beijing, China) according to the manufacturer's protocol. Protein contents were determined in nuclear and cytosol fractions supernatants, and Western blotting was conducted as described above.

2.11. *Real-time polymerase chain reaction (RT-PCR)*

The TRIzol reagent (Transgen, Beijing, China) was used to extract total RNA, and the RNA contents were assessed by a Nanodrop 2000 Spectrophotometer (Thermo Fisher Scientific). One microgram of total RNA was used for cDNA synthesis with a reverse transcription kit (Transgen), according to the manufacturer's instructions. The cDNA was amplified by a LightCycler 480 System II (Roche Applied Science, Indianapolis, IN, USA) using an SYBR Green I PCR master kit (Transgen). Reaction mixtures were incubated for 40 amplification cycles as follows: degeneration at 95 °C for 15 s; extension at 55 °C for 30 s; and annealing at 72 °C for 20 s. The relative expression levels of the target genes were normalized to the level of *Gapdh* using the $2^{-\Delta\Delta CT}$ method. All primers used in the experiment are shown in Table 1.

2.12. *MiRNA determination*

For quantification of the various miRNA levels, cDNAs were synthesized using a reverse transcription kit (RiboBio, Guangzhou, China) in accordance with the manufacturer's instructions. Then, the amplification of miRNA was performed with the specific primers using the LightCycler 480 System II (Roche Applied Science) under the standard conditions. The relative miRNA concentration was quantified as the ratio between the expression of miRNA and the endogenous control U6.

2.13. *Cell transfection*

Transfection was performed using Lipofectamine 3000 transfection agent (Invitrogen, Grand Island, NY, USA) according to the manufacturer's instructions. Then, RAW264.7 or 293T cells were transfected with miR-155 mimic (50 nmol/L) or a negative control (NC) designed and provided by RiboBio. After transfection, the media were substituted with fresh incubation media containing FBS (BI), and the cells were incubated at a 37 °C and 5% CO_2 incubator for 6 h. Then, the cells were stimulated with LPS (1 μg/mL) and incubated with YD for 48 h. For each variant, three independent transfections were performed.

Table 1 Primer sequences used for semi-quantitative RT-PCR analyses. F, forward; R: reverse.

Gene	Primer sequence (5′−3′)
α-Sma-F	ACTGGGACGACATGGAAAAG
α-Sma-R	CATCTCCAGAGTCCAGCACA
Tgf-β-F	ATGGTGGACCGCAACAAC
Tgf-β-R	CCAAGGTAACGCCAGGAA
Col1a1-F	GCTCCTCTTAGGGGCCACT
Col1a1-R	CCACGTCTCACCATTGGGG
Ctgf-F	GGGCCTCTTCTGCGATTTC
Ctgf-R	ATCCAGGCAAGTGCATTGGTA
Timp1-F	GCAACTCGGACCTGGTCATAA
Timp1-R	CGGCCCGTGATGAGAAACT
Il-1β-F	GCAACTGTTCCTGAACTCAACT
Il-1β-R	ATCTTTTGGGGTCCGTCAACT
iNos-F	GTTCTCAGCCCAACAATACAAGA
iNos-R	GTGGACGGGTCGATGTCAC
Tnf-α-F	CCCTCACACTCAGATCATCTTCT
Tnf-α-R	GCTACGACGTGGGCTACAG
Mcp-1-F	TTAAAAACCTGGATCGGAACCAA
Mcp-1-R	GCATTAGCTTCAGATTTACGGGT
Casp12-F	AGACAGAGTTAATGCAGTTTGCT
Casp12-R	TTCACCCCACAGATTCCTTCC
Gapdh-F	AGGTCGGTGTGAACGGATTTG
Gapdh-R	TGTAGACCATGTAGTTGAGGTCA

2.14. *Dual-luciferase reporter assay*

The wild-type (WT) 3′ UTR sequence of *Casp12* containing the predicted target sites of miR-155 and the mutant (MUT) sequence were offered by RiboBio. The 293T cells were co-transfected with miR-155 mimic, NC and *Casp12*-3′ UTR-luciferase WT plasmids, or *Casp12*-3′ UTR-luciferase MUT plasmids by Lipofectamine 3000 transfection agent in a 96-well plate. Luciferase activity was measured by a dual-luciferase reporter assay kit (Promega, Madison, WI, USA) after the incubation for 48 h. The relative expression levels were normalized to the *Renilla* luciferase activity. The analyses were performed three times.

2.15. *Immunofluorescence*

RAW264.7 cells were subjected to a series of treatments and immobilized with 4% paraformaldehyde (Beyotime) at room temperature for 0.5 h. Then, the cells were permeabilized with 0.1% Triton X-100 (Merck) diluted in PBS for 10 min. After being blocked with 10% BSA for 1 h at 37 °C, the cells were incubated with P65 antibody (1:200) at 4 °C overnight. The cells were incubated with secondary antibody conjugated to Alexa Fluor 488 (1:10,000, Abcam) for 1 h at room temperature. Then, Hoechst 33342 was used to counterstain the nucleus at room temperature for 10 min. Signal of the intracellular fluorescence was assessed

by a Confocal Laser Scanning Microscope System (FV3000, Olympus, Tokyo, Japan).

2.16. Statistical analyses

The analyses of all experiments were performed with three biological replicates. All values are presented as the mean ± standard deviation (SD). The experimental data were analyzed by one-way ANOVA followed by Tukey's multiple comparison test using GraphPad Prism Version 7 (GraphPad Software, La Jolla, CA, USA). Differences were considered statistically significant for *P*-values below 0.05.

3. Results

3.1. YD ameliorated CCl_4-induced liver injury

To determine whether YD has a liver protective effect on the chronic CCl_4-induced liver fibrosis murine model, we evaluated the levels of structural damage and liver function. In the liver morphology analyses (Fig. 1B), the livers of the CCl_4-induced mice exhibited faded-color changes, and these changes were partially reversed by YD treatments. Histological analyses with H&E staining (Fig. 1B) show that the liver tissues and the hepatocytes were normal in the oil group, and the extensive hepatocyte edema, acidophilic changes, and significant lymphocyte infiltration in the portal area of the lobule were observed in the CCl_4-treated mice. And YD treatment alleviated the pathological changes in the liver tissues. We did not observe a significant effect on the ratio of liver weight to body weight in the mice after administration of YD (Fig. 1C). Then, we assessed serum markers of hepatocellular damage. As shown in Fig. 1D and E, the levels of ALT and AST were obviously elevated in the CCl_4-induced group in comparison with the oil group. And YD treatment decreased the levels of these biomarkers. Collectively, YD ameliorates liver injury in CCl_4-induced mice.

3.2. YD alleviated collagen accumulation and hepatic stellate cell (HSC) activation

To further confirm the inhibitory effects of YD on liver fibrosis, collagen deposition was detected by Sirius red staining. We found that the collagen deposition of mice in CCl_4-induced group was significantly increased compared with that in oil group, while YD treatment obviously reduced the collagen deposition induced by CCl_4 injection (Fig. 2A). Then, we assessed markers of liver fibrogenesis by performing immunohistochemistry staining to detect the expression of Col1a1 and α-SMA in the liver tissues. The results in Fig. 2A show that CCl_4 increased the α-SMA and Col1a1 levels in CCl_4-treated mice. In contrast, these effects were partially reversed by YD. The protein expression levels of α-SMA and Col1a1 in tissues were analyzed by Western blotting, and the results also reveal that YD could reduce collagen deposition (Fig. 2E and F). RT-PCR analyses of the expression of fibrotic factors in the tissues, including *α-Sma*, *Col1a1*, tissue inhibitor of metalloproteinases 1 (*Timp1*), connective tissue growth factor (*Ctgf*), and transforming growth factor beta (*Tgf-β*), also show the same results as those of immunohistochemistry staining and Western blotting (Fig. 2G). Furthermore, the results of CCK-8 assay shown in Supporting Information Fig. S1A and S1B demonstrate that YD did not have toxic effects on the human HSC line LX-2 and the human normal liver cell line LO2 cells. We also measured the protein expression of α-SMA and Col1a1 in LX-2 cells and found that these proteins were inhibited by YD treatments (Fig. 2H and I). Overall, these results show that YD ameliorates collagen accumulation and HSC activation.

3.3. Effects of YD on miR-155 expression

To gain insight into the expression changes of various miRNAs by YD during liver fibrosis, we screened several miRNAs associated with liver fibrosis and inflammation in mice by RT-PCR, including miR-125, miR-155, let-7a, miR-150, and miR-146[15–17]. As shown in Supporting Information Fig. S2, we chose miR-155 for subsequent experiments because its expression was substantially increased in CCl_4-induced mice ($P < 0.001$), and this increase was significantly prevented by YD administration ($P < 0.01$).

As one of the most important miRNAs during liver fibrosis and inflammation, miR-155 is a target of intense research, which may result in the identification of novel antifibrotic approaches[8,18]. To determine whether YD could modulate miR-155 expression, we measured the miR-155 levels *in vivo* and *in vitro*. As shown in Fig. 3A, CCl_4 stimulation significantly increased the miR-155 levels in mice compared with those of the oil group. And YD could partially reverse the expression of miR-155. Similar results were also observed in LPS-induced RAW264.7 cells (Fig. 3B). YD downregulated the miR-155 expression *in vitro*. Meanwhile, YD had no toxic effect on RAW264.7 cells as shown by CCK-8 assays (Supporting Information Fig. S1C). Furthermore, transfection of RAW264.7 cells with the miR-155 mimic significantly increased miR-155 levels in RAW264.7 cells compared with those of the miR-NC group (Supporting Information Fig. S3), indicating a successful transfection.

3.4. Casp12 is a novel direct target of miR-155

Given that miR-155 has tremendously important effects on the progression of liver fibrosis, we first needed to identify the targets of miR-155 in liver fibrosis and inflammation. Thus, we searched for possible targets of miR-155 by TargetScan[19]. In this database, there are 430 shared predicted target genes of miR-155. Given that miR-155 promotes liver fibrosis and inflammation, we assessed the regulation of five possible target genes by miR-155, including suppressor of cytokine signaling 1 (*Sosc1*), inositol polyphosphate-5-phosphatase D (*Ship1*), *Nrf2*, *Casp12*, and protein tyrosine phosphatase non-receptor type 2 (*Ptpn2*). We examined the mRNA expression of these genes by RT-PCR analyses in the liver tissues (Supporting Information Fig. S4). Only the mRNA levels of *Casp12*, *Ship1*, *Sosc1*, and *Nrf2* were decreased in the CCl_4-induced mice, and they were increased following YD administration, which suggested that they may be the targets of miR-155. Since *Ship1*, *Sosc1*, and *Nrf2* had been proven to be the targets of miR-155, we only focused on the novel target, *Casp12*, in liver fibrosis.

Western blotting analyses of whole liver samples reveal that the CASP12 protein levels were downregulated after CCl_4 injection compared with those of the control livers, and could be partially reversed by YD administration (Fig. 4A). Similar beneficial effects were confirmed in LPS-induced RAW264.7 cells by Western blotting (Fig. 4B). The gene expression levels of *Casp12* determined by RT-PCR in CCl_4-induced mice (Fig. 4C) and LPS-induced RAW264.7 cells (Fig. 4D) coincided with the results of Western blotting.

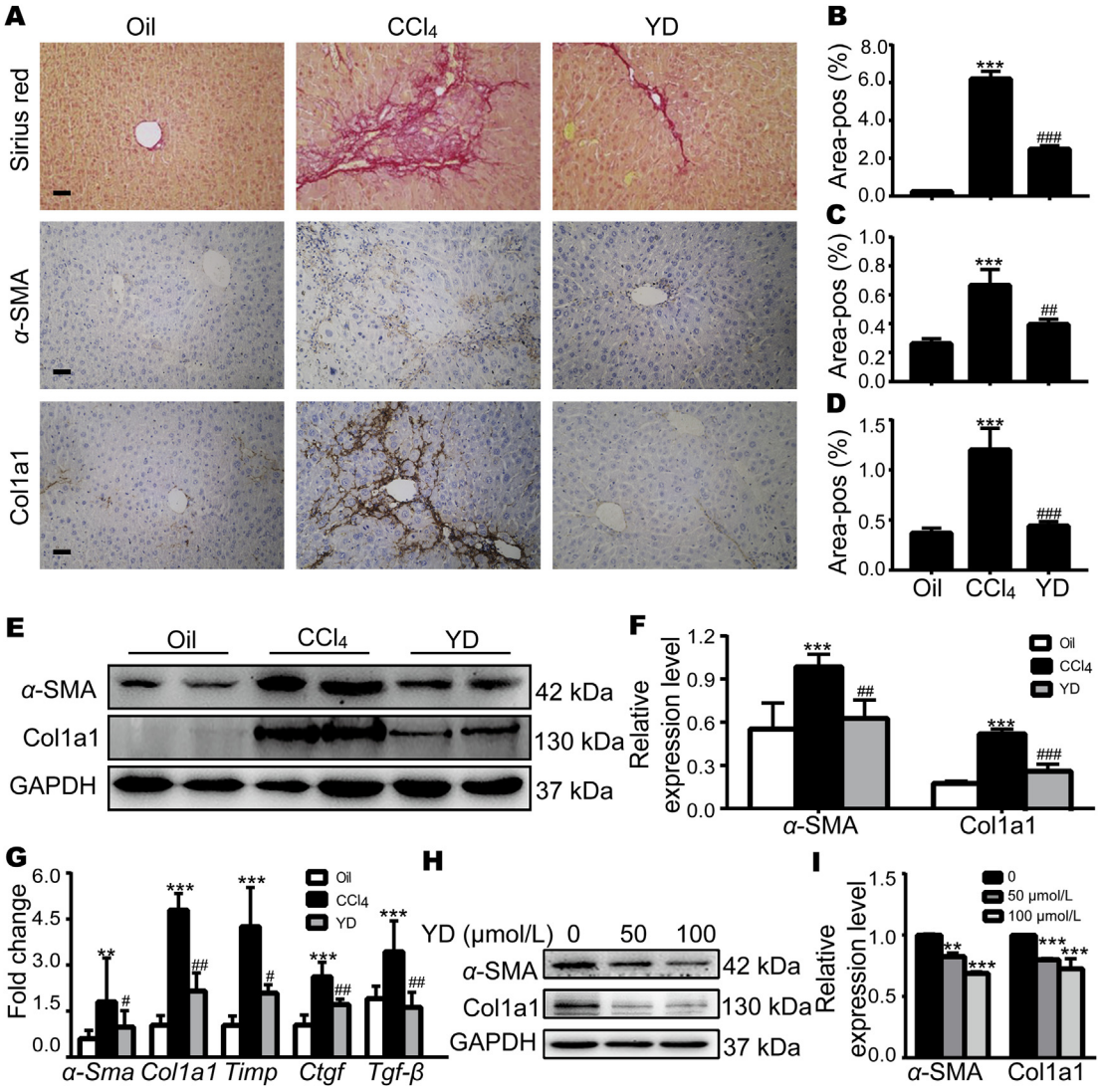

Figure 2 YD alleviated collagen accumulation and hepatic stellate cell (HSC) activation. (A) The representative photos of liver specimens with Sirius red staining and immunohistochemical staining for α-smooth muscle actin (α-SMA) and collagen type I alpha 1 (Col1a1) in oil or CCl_4-induced mice with or without YD administration ($n = 6$/group). Liver tissues were observed by microscopy (scale bar, 50 μm). (B)−(D) Positive staining area analyses of the histological images shown in A (mean ± SD, $n = 6$). (E) Western blotting analyses of α-SMA and Col1a1 in mice. (F) Densitometric analyses of the blots shown in E (mean ± SD, $n = 6$). (G) RT-PCR analyses of genes involved in liver fibrogenesis, including *α-Sma*, *Col1a1*, *Timp1*, *Ctgf*, and *Tgf-β* (mean ± SD, $n = 6$). (H) Western blotting analyses for α-SMA and Col1a1 in LX-2 cells. (I) Densitometric analyses of the blots shown in H (mean ± SD, $n = 3$). $^{**}P < 0.01$, $^{***}P < 0.001$ *vs.* the oil or control; $^{\#}P < 0.05$, $^{\#\#}P < 0.01$, $^{\#\#\#}P < 0.001$ *vs.* the CCl_4-induced group. Area-pos, the area of positive staining; *Timp1*, tissue inhibitor of metalloproteinases 1; *Ctgf*, connective tissue growth factor; *Tgf-β*, transforming growth factor beta.

According to the results of Fig. 4B and D, we selected the 50 μmol/L concentration of YD for the subsequent rescue experiment. To confirm the direct relationship between miR-155 and *Casp12*, we searched for a potential miR-155 binding site in the *Casp12* 3′ UTR by TargetScan (Fig. 4E). Then, we performed a dual luciferase reporter assay to verify the binding relationship, and the luciferase activity was significantly reduced when miR-155 targeted WT *Casp12* compared with the NC group (Fig. 4F). Furthermore, the Western blotting results show that CASP12 was significantly decreased in miR-155 mimic transfected RAW264.7 cells, and after the administration of YD, there was no difference in the levels of CASP12 (Fig. 4G). These data indicat that *Casp12* is a direct target gene of miR-155 and that YD upregulates the levels of *Casp12* by inhibiting miR-155.

3.5. *YD inhibited inflammation during liver fibrosis via miR-155*

Previous studies demonstrated that YD possesses antibacterial activity and antioxidant potential[13,14]. These characteristics are closely related to the inflammatory responses. Therefore, we next investigated the inhibitory effects of YD on liver inflammation. As shown in Fig. 5A, immunohistochemistry results reveal that the positive staining of CD68, a macrophage activation marker, substantially increased in the liver after CCl_4 induction compared to that of control mice. This increase was partially suppressed by YD treatment. RT-PCR analyses of the inflammation-related genes in the liver tissues also demonstrate that YD inhibited the expression of inflammatory factors (Fig. 5B). ELISA results further show that YD significantly reduced the secretion of TNF-α and IL-1β in

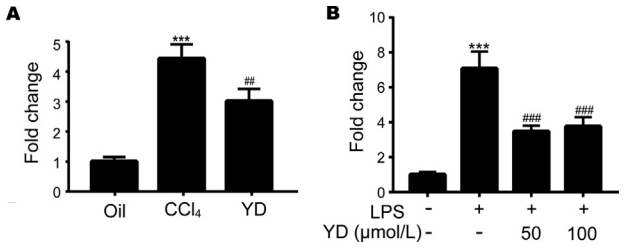

Figure 3 Effects of YD on miR-155 expression. (A) YD inhibited the expression of miR-155 in the CCl_4-induced mice (mean ± SD, $n = 6$). $^{***}P < 0.001$ *vs.* the oil group; $^{\#\#}P < 0.01$ *vs.* the CCl_4-induced group. (B) YD inhibited the expression of miR-155 in the lipopolysaccharide (LPS)-induced RAW264.7 cells (mean ± SD, $n = 3$). $^{***}P < 0.001$ *vs.* control; $^{\#\#\#}P < 0.001$ *vs.* LPS-induced group (without YD).

serum (Fig. 5C and D). As shown in Fig. 5E, the results of protein expression of TNF-α in mice were coincided with those of mRNA expression. Meanwhile, Western blotting results of LPS-induced RAW264.7 cells show that YD inhibited the expression of TNF-α and IL-1β (Supporting Information Fig. S5). Additionally, to further verify the anti-inflammatory role of YD *via* miR-155, we used LPS to activate RAW264.7 cells, and the protein level of TNF-α was analyzed by Western blotting in LPS-activated RAW264.7 cells with overexpressing miR-155 mimic or its control (Fig. 5F). As expected, the LPS-mediated increase in TNF-α protein expression was restored by YD treatment. However, we failed to observe significant differences in miR-155 mimic transfected cells treated with or without YD. Furthermore, the results of the content-detection of TNF-α *in vitro* by ELISA were consistent with the findings of Western blotting (Fig. 5G). These data demonstrate that YD exerts anti-inflammatory effects *via* inhibiting miR-155.

3.6. *Effects of YD on the NF-κB pathway*

As one of the most important signaling pathways of inflammation, NF-κB pathway controls a wide variety of cellular programs, and it can be activated *via* phosphorylation of IκB kinase (IKK). The observation that YD treatment inhibits inflammation impelled us to survey whether YD affects the NF-κB pathway. As shown in Fig. 6A, pretreatment with YD distinctly blocked the CCl_4-induced upregulation of the phosphorylation of the IKKβ, IκBα, and P65 proteins. Parallel results were confirmed in LPS-induced RAW264.7 cells by Western blotting (Fig. 6B), LPS enhanced IKKβ, IκBα, and P65 phosphorylation, which was largely reversed by YD. Furthermore, to investigate whether P65 nuclear translocation is involved in the effects of YD, we performed Western blotting to examine whether YD affects the cytosolic and nuclear P65 protein expression in cells (Fig. 6C). After incubating with LPS, nuclear P65 protein expression levels were enhanced while cytosolic P65 protein expression levels were decreased, compared with those of the vehicle-treated control group, and administration of YD yielded in the opposite results. YD significantly inhibited the translocation of P65 from the cytoplasm to the nucleus. Additionally, we performed immunofluorescence staining assays of P65 in the cytoplasm and nuclei of RAW264.7 cells (Fig. 6D), in accordance with the above data, after treatment with YD, the translocation of P65 from the cytoplasm to the nucleus was inhibited, and the inhibitory effect was reduced in miR-155-mimic-transfected cells. We failed to observe significant differences in the group treated with YD. These data demonstrate that YD inhibits the NF-κB pathway *via* miR-155.

4. Discussion

Hepatic fibrosis is a pathological hallmark of the deterioration of different underlying chronic liver diseases resulting from long-standing liver injuries and represents one of the major health care burdens worldwide[20], which have a high mortality rate and incidence[21,22]. During liver fibrogenesis, the liver parenchyma is progressively substituted with scar tissue characterized by excessive accumulation of fibrillar ECM. If untreated, liver fibrosis results in the loss of liver function and cirrhosis, which can have a poor outcome and high mortality[23]. To date, no appropriate drug treatments are available clinically. Here, we found that YD has favorable characteristics for the treatment of CCl_4-induced liver fibrosis and LX-2 cells. To our knowledge, this is the first study to show a significant association between the antimicrobial peptide and liver fibrosis. Firstly, we showed that the antimicrobial peptide YD is an effective antifibrotic candidate that inhibits ECM production and α-SMA expression, and improves liver function. Secondly, we found that YD attenuates liver fibrosis *in vitro* and *in vivo*, at least in part, *via* suppressing inflammation. The inhibition of inflammation in RAW264.7 cells and CCl_4-treated mice was associated with the suppression of the NF-κB pathway, as indicated by YD mediated reductions in the phosphorylation levels of IKKβ, IκBα, and P65, and inhibited P65 nuclear translocation. Finally, our results proved for the first time that YD could decrease miR-155 expression and that *Casp12* is a new target of miR-155, as shown by the bioinformatics analyses and verified by luciferase assays. Taken together, these results indicate that the antimicrobial peptide YD downregulates inflammation through meditating the miR-155−*Casp12*−NF-κB axis during liver fibrosis (Fig. 7). The findings of the current study may provide a novel therapeutic candidate and target in liver fibrosis.

Substantial evidence indicates a link between inflammation and liver fibrogenesis, and tissue damage and inflammation are important triggers for fibrosis[24]. Macrophages play an important role in the pathogenesis of hepatic injury and subsequent fibrosis[25], and they possess the ability to promote or inhibit inflammation and fibrosis depending on their activation state[26]. Activated macrophages have been shown to directly promote interstitial fibrosis *via* the production of profibrotic factors, such as transforming growth factor-β (TGF-β)[27], and indirectly activate HSCs, resulting in the formation of ECM components[28], which are involved in the pathogenesis of hepatic fibrosis *via* increasing the expression of proinflammatory cytokines[29]. Inflammation control-based therapy has emerged as a new therapeutic strategy.

Antimicrobial peptides (AMPs), new antimicrobial molecules that counteract bacterial infections, have attracted increasing attention because of their broad antimicrobial activity and specific antimicrobial mechanism[30]. AMPs are therapeutic in several disease models because they possess immunomodulatory properties *via* mediating a series of processes, including inflammatory responses, chemoattraction, activation of innate and adaptive compartments, wound healing, autophagy, and apoptosis[31]. All of these functions simultaneously drive the antibacterial and anti-inflammatory activities of AMPs. A very recent report from Zhai et al.[32] suggested that cecropin A alleviates inflammation by modulating the gut microbiota in mice with inflammatory bowel

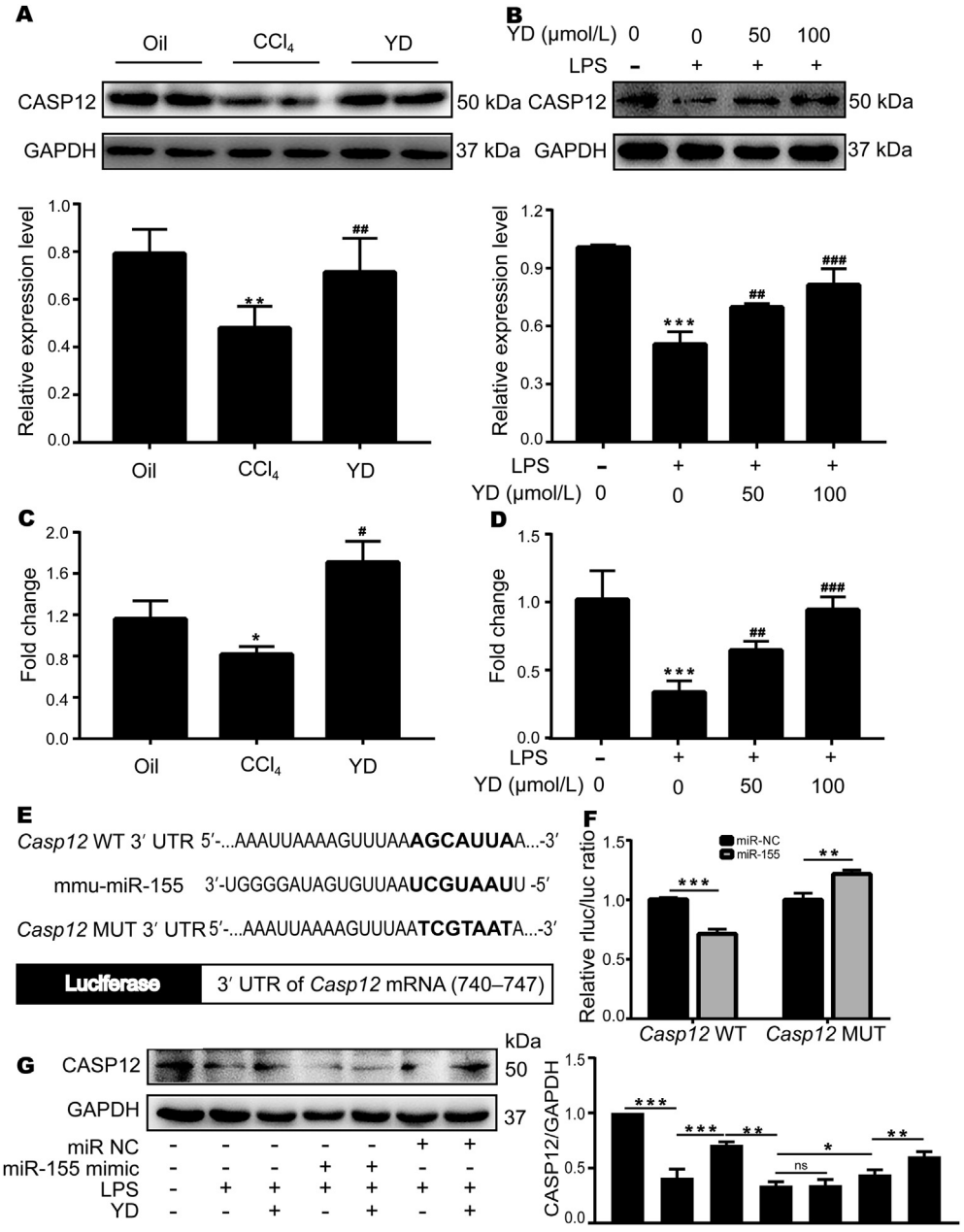

Figure 4 *Casp12* is a novel direct target of miR-155. (A) Immunoblotting and statistical analyses of CASP12 in CCl_4-induced mice after administration of YD (mean ± SD, $n = 6$). $^{**}P < 0.01$ *vs.* the oil group; $^{\#\#}P < 0.01$ *vs.* the CCl_4-induced group. (B) Immunoblotting and statistical analyses of CASP12 in LPS-induced RAW264.7 cells after administration of YD (mean ± SD, $n = 3$). $^{***}P < 0.001$ *vs.* control; $^{\#\#}P < 0.01$, $^{\#\#\#}P < 0.001$ *vs.* LPS-induced group (without YD). (C) The results of RT-PCR analyses of *Casp12* in the CCl_4-induced mice after administration of YD (mean ± SD, $n = 6$). $^{*}P < 0.05$ *vs.* the oil group; $^{\#}P < 0.05$ *vs.* the CCl_4-induced group. (D) The results of RT-PCR analyses of *Casp12* in the LPS-induced RAW264.7 cells after administration of YD (mean ± SD, $n = 3$). $^{***}P < 0.001$ *vs.* control; $^{\#\#}P < 0.01$, $^{\#\#\#}P < 0.001$ *vs.* LPS-induced group (without YD). (E) Binding sites of *Casp12* and miR-155 were predicted by TargetScan. The bold letters represent putative miR-155 target binding sites in the *Casp12* 3′ UTR. (F) Luciferase reporter analysis was utilized to confirm the binding between miR-155 and *Casp12*. The relative luciferase activity was normalized to *Renilla* activity. $^{**}P < 0.01$, $^{***}P < 0.001$ *vs.* miR-NC. (G) The protein expression levels of CASP12 in cells overexpressing miR-155 mimic or its control were analyzed by Western blotting and densitometric analyses. $^{*}P < 0.05$, $^{**}P < 0.01$, $^{***}P < 0.001$, ns: no significant differences.

disease. Haney et al.[33] analyzed the effect of aggregation on the immunomodulatory activity of synthetic innate defense regulator peptides. In Liu et al.'s study[34], the peptide FFW showed proapoptotic and antimigratory effects in hepatocellular carcinoma cells. While numerous studies have focused on the antimicrobial activity of these molecules, little is known about their influence on liver fibrosis. Our results show that YD treatment significantly improved liver function and decreased the collagen and α-SMA contents, suggesting that YD partially alleviates CCl_4-induced liver fibrosis. To the best of our knowledge, no studies have examined the role of AMPs in CCl_4-induced liver fibrosis. Our work provides new insights into the role of AMPs in liver fibrosis.

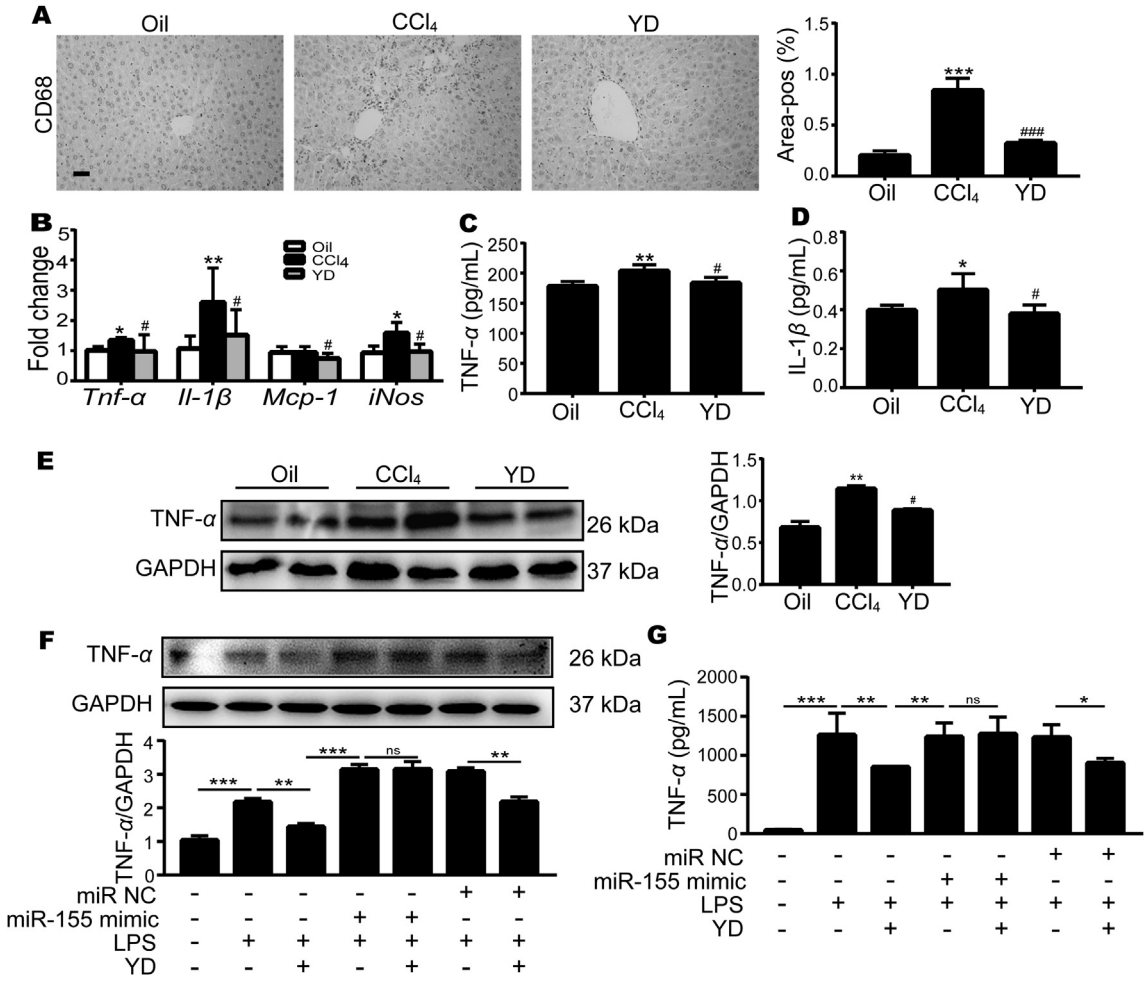

Figure 5 The effects of YD on inflammation during liver fibrosis *via* miR-155. (A) The representative photos of liver specimens with immunohistochemical staining for CD68, and positive staining area analyses of the histological images (scale bar, 50 μm; mean ± SD, $n = 6$). $^{***}P < 0.001$ *vs.* the oil group; $^{\#\#}P < 0.01$ *vs.* the CCl_4-induced group. (B) RT-PCR analyses of genes involved in inflammation, including *Tnf-α*, *Il-1β*, *Mcp-1*, and *iNos* (mean ± SD, $n = 6$). $^{*}P < 0.05$, $^{**}P < 0.01$ *vs.* the oil group; $^{\#}P < 0.05$ *vs.* the CCl_4-induced group. (C) and (D) ELISA analyses of TNF-α and IL-1β in serum (mean ± SD, $n = 6$). $^{*}P < 0.05$, $^{**}P < 0.01$ *vs.* the oil group; $^{\#}P < 0.05$ *vs.* the CCl_4-induced group. (E) Western blotting and densitometric analyses of TNF-α in mice. (F) The TNF-α protein levels in cells overexpressing miR-155 mimic or its control were analyzed by Western blotting and densitometric analysis (mean ± SD, $n = 3$). $^{**}P < 0.01$, $^{***}P < 0.001$, ns: no significant differences. (G) The concentration of TNF-α in cells overexpressing miR-155 mimic or its control was detected by ELISA (mean ± SD, $n = 3$). $^{*}P < 0.05$, $^{**}P < 0.01$, $^{***}P < 0.001$, ns: no significant differences. *Tnf-α*, tumor necrosis factor alpha; *Il-1β*, interleukin-1 beta; *Mcp-1*, monocyte chemoattractant protein-1; *iNos*, inducible nitric oxide synthase.

MiRNAs, a group of endogenous small (18−22 nt) non-coding RNA fragments, play essential roles in numerous biological processes, including cell proliferation, differentiation, apoptosis, and metabolism[35]. Emerging studies have indicated that miRNAs regulate the progression of liver fibrosis by inhibiting their target gene's mRNAs, and abnormal expression of miRNAs is closely related to the initiation and progression of hepatic fibrosis[36]. MiR-155, universally expressed in several tissues and cell types, is involved in inflammation and linked with liver diseases[18]. A recent study reported that miR-155 promotes liver fibrosis and steatohepatitis by increasing the levels of peroxisome proliferator-activated receptors and peroxisome proliferator-activated receptor response elements[8]. In addition, miR-155 has emerged as a molecular target of some inflammation-related diseases through targeting gene suppressor of cytokine signaling 1 (SOCS1) or SH2 domain-containing inositol 5-phosphatase 1 (SHIP1), which are known to regulate the NF-κB signaling pathway[37,38]. In this study, we found that the inflammatory factors and the expression of miR-155 were upregulated in CCl_4-induced mice and LPS-induced RAW264.7 cells. However, these elevations were significantly inhibited by YD administration. Furthermore, we demonstrate that *Casp12* is a novel target of miR-155 and hypothesized that the anti-inflammatory effect of YD during liver fibrosis occurs *via* miR-155-mediated *Casp12*. In support of this hypothesis, we show that overexpression of miR-155 repressed the expression of CASP12, but this decrease was attenuated by YD in RAW264.7 cells. However, the cellular source of miR-155 decrease after YD treatment and the mechanism underlying the direct regulation of miR-155 by YD are still not clear, and further studies are warranted to identify the cellular source of miR-155 by isolating primary cells from mice[39] and explore the transcription factors that regulating miR-155[40].

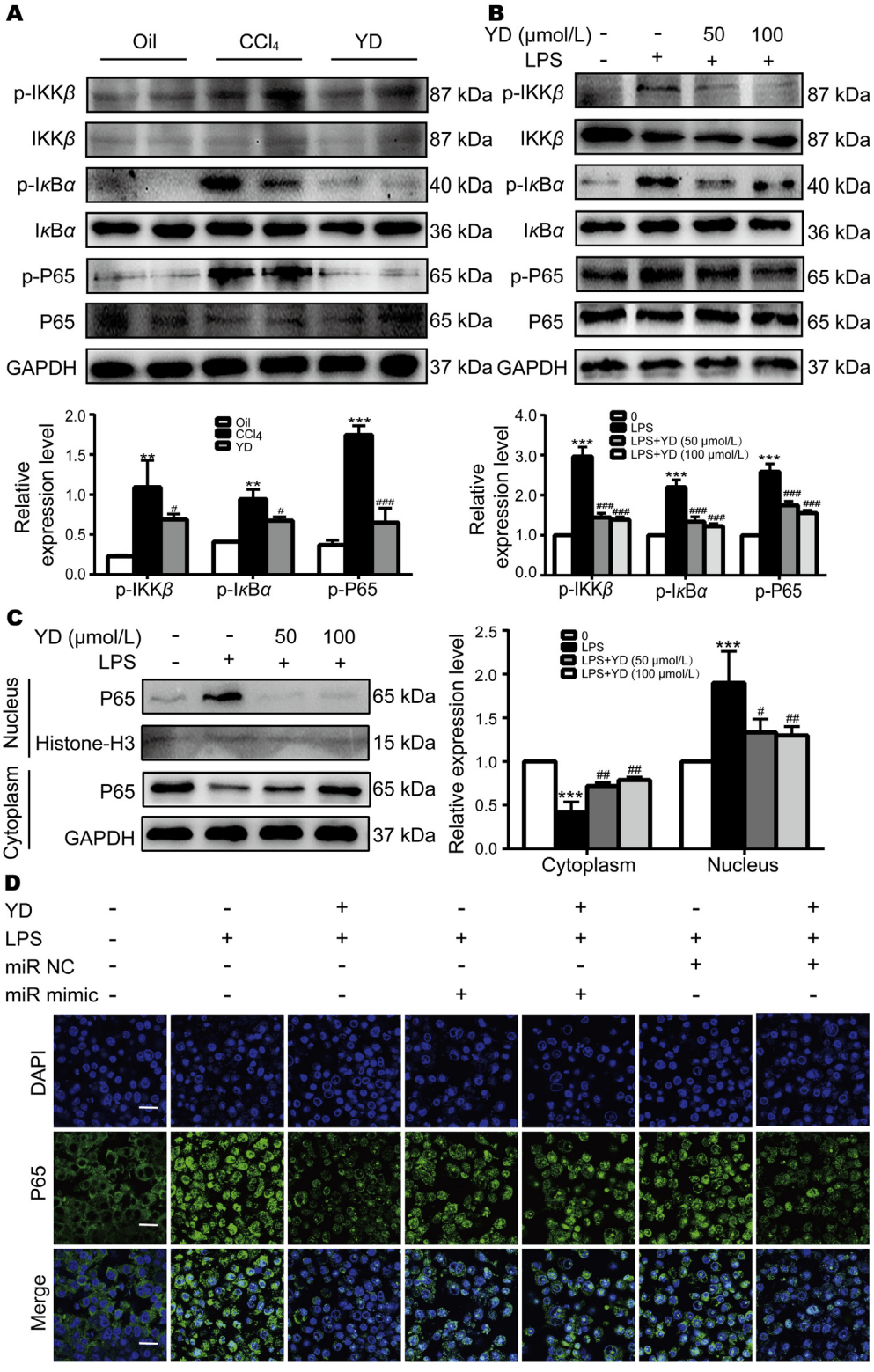

Figure 6 YD significantly inhibited NF-κB pathway *in vivo* and *in vitro*. (A) YD inhibited NF-κB pathway in the CCl_4-induced mice (mean ± SD, $n = 6$). $^{**}P < 0.01$, $^{***}P < 0.001$ *vs.* the oil group; $^{\#}P < 0.05$, $^{\#\#\#}P < 0.001$ *vs.* the CCl_4-induced group. (B) YD inhibited NF-κB pathway in the LPS-induced RAW264.7 cells (mean ± SD, $n = 3$). $^{***}P < 0.001$ *vs.* control; $^{\#\#\#}P < 0.001$ *vs.* LPS-induced group (without YD). (C) The protein expression levels of P65 in the cytosol and nucleus were examined by Western blotting (mean ± SD, $n = 3$). Histone-H3 is an internal reference indicator of the nucleus, and the nucleus protein expression levels are normalized to Histone-H3 levels. $^{***}P < 0.001$ *vs.* control; $^{\#}P < 0.05$, $^{\#\#}P < 0.01$ *vs.* LPS-induced group (without YD). (D) Nuclear translocation of P65 in RAW264.7 cells with overexpressing miR-155 mimic or its control was assayed by immunofluorescence (scale bar, 20 μm).

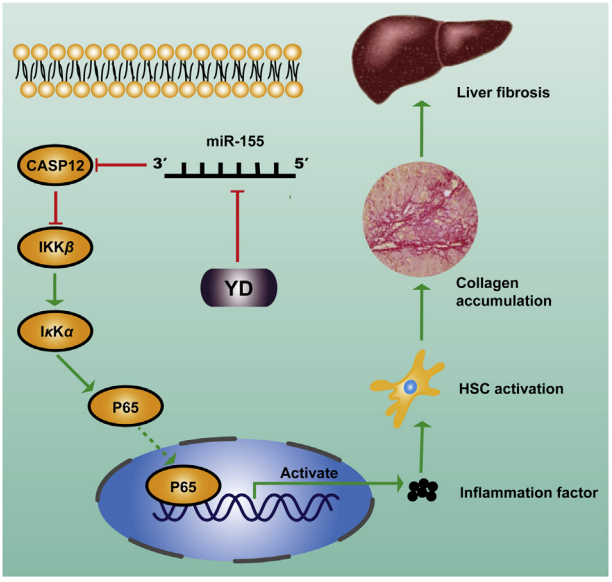

Figure 7 Schematic of the mechanism underlying the YD inhibition of hepatic fibrosis development. YD could decrease miR-155 expression, which is responsible for the upregulation of CASP12, leading to the decreased secretion of inflammatory cytokines *via* inactivation of NF-κB pathway, and finally inhibit the development of fibrosis. Green arrows indicate the facilitation of this process, whereas red blocks represent the inhibition of this process.

CASP12, a member of the caspase-1 subfamily, mediates the proteolytic activation of inflammatory cytokines and has a negative regulatory effect on the inflammasome and NF-κB pathway[41,42]. LeBlanc et al.[43] demonstrated that CASP12 inhibits NF-κB activation by displacing Traf6 from the signaling complex and binding to Rip2 in knockout mice. Another report from the same group elegantly showed that CASP12 inhibited the activation of NF-κB signaling pathway through competing with the NF-κB essential modulator in combination with IKK, successfully blocking the production of the IKK complex[41]. Consistent with our own observations, in our analyses, CASP12 induced by YD in liver fibrosis seems to be a powerful effector that inhibits the inflammation-activating process. YD increased the CASP12 expression level and repressed the inflammatory response, as demonstrated by YD reducing the release of inflammatory cytokines and blunting the activation phenotype of NF-κB *via* inhibition of IKKβ, IκBα, and P65 phosphorylation. These results suggest a possible mechanism whereby CASP12 production is induced by YD-decreased miR-155 to inhibit inflammation during liver fibrosis. Interestingly, because previously reported *Casp12* knockout mice also lack CASP11 expression[42], a comment from Vande Walle et al.[44] raised the question of whether CASP12 suppresses inflammasome activation. Therefore, future research is needed to determine whether YD affects liver fibrosis through regulating CASP12.

5. Conclusions

Our findings show that the anti-inflammatory effects of the antimicrobial peptide YD are beneficial for alleviating liver fibrosis. Furthermore, the inhibitory role of YD in inflammatory responses is mediated by the miR-155−*Casp12*−NF-κB axis (Fig. 7). This specificity suggests that antimicrobial peptides have potential utility for therapeutic use in combating liver fibrosis.

Acknowledgments

This work was supported by the National Natural Science Foundation of China (No. 81602945, 81673283, and 81874315), the CAMS Innovation Fund for Medical Sciences (CIFMS, No. 2019-I2M-5-074, China) and the Program for the Ministry of Education "Peptide Drugs" Innovation Team (No. IRT_15R27, China).

Author contributions

Junqiu Xie and Xianxing Jiang contributed to the design of the research and provided financial support; Zhibin Yan performed the experiments and analyzed the data; Dan Wang, Chunmei An, and Hongjiao Xu helped to perform the cellular experiments; Qian Zhao, Ying Shi, and Nazi Song helped to perform the animal experiments; Bochuan Deng and Xiaomin Guo conducted some other experiments; Jing Rao and Lu Cheng helped to analyze the data; Bangzhi Zhang, Lingyun Mou, and Wenle Yang revised the manuscript.

Conflicts of interest

The authors declare that they have no financial or non-financial potential conflicts of interest.

Appendix A. Supporting information

Supporting data to this article can be found online at https://doi.org/10.1016/j.apsb.2020.07.004.

References

1. Tacke F, Trautwein C. Mechanisms of liver fibrosis resolution. *J Hepatol* 2015;**63**:1038−9.
2. Kaffe E, Katsifa A, Xylourgidis N, Ninou I, Zannikou M, Harokopos V, et al. Hepatocyte autotaxin expression promotes liver fibrosis and cancer. *Hepatology* 2017;**65**:1369−83.
3. Kang JW, Hong JM, Lee SM. Melatonin enhances mitophagy and mitochondrial biogenesis in rats with carbon tetrachloride-induced liver fibrosis. *J Pineal Res* 2016;**60**:383−93.
4. Li X, Tian Y, Tu MJ, Ho PY, Batra N, Yu AM. Bioengineered miR-27b-3p and miR-328-3p modulate drug metabolism and disposition *via* the regulation of target ADME gene expression. *Acta Pharm Sin B* 2019;**9**:639−47.
5. Sonkoly E, Pivarcsi A. MicroRNAs in inflammation. *Int Rev Immunol* 2009;**28**:535−61.
6. Wu X, Wang Y, Yu T, Nie E, Hu Q, Wu W, et al. Blocking MIR155HG/miR-155 axis inhibits mesenchymal transition in glioma. *Neuro Oncol* 2017;**19**:1195−205.
7. Zhao R, Dong R, Yang Y, Wang Y, Ma J, Wang J, et al. MicroRNA-155 modulates bile duct inflammation by targeting the suppressor of cytokine signaling 1 in biliary atresia. *Pediatr Res* 2017;**82**:1007−16.
8. Bala S, Csak T, Saha B, Zatsiorsky J, Kodys K, Catalano D, et al. The pro-inflammatory effects of miR-155 promote liver fibrosis and alcohol-induced steatohepatitis. *J Hepatol* 2016;**64**:1378−87.
9. Heymans S, Corsten MF, Verhesen W, Carai P, van Leeuwen RE, Custers K, et al. Macrophage microRNA-155 promotes cardiac hypertrophy and failure. *Circulation* 2013;**128**:1420−32.

10. Hu J, Huang CX, Rao PP, Cao GQ, Zhang Y, Zhou JP, et al. MicroRNA-155 inhibition attenuates endoplasmic reticulum stress-induced cardiomyocyte apoptosis following myocardial infarction *via* reducing macrophage inflammation. *Eur J Pharmacol* 2019;**857**:172449.
11. Artlett CM, Sassi-Gaha S, Hope JL, Feghali-Bostwick CA, Katsikis PD. Mir-155 is overexpressed in systemic sclerosis fibroblasts and is required for NLRP3 inflammasome-mediated collagen synthesis during fibrosis. *Arthritis Res Ther* 2017;**19**:144.
12. Li HD, Du XS, Huang HM, Chen X, Yang Y, Huang C, et al. Non-coding RNAs in alcoholic liver disease. *J Cell Physiol* 2019;**234**:14709−20.
13. Rahman MS, Choi YH, Choi YS, Yoo JC. Glycin-rich antimicrobial peptide YD1 from *B. amyloliquefaciens*, induced morphological alteration in and showed affinity for plasmid DNA of *E. coli*. *AMB Express* 2017;**7**:8.
14. Rahman MS, Hee Choi Y, Seok Choi Y, Alam MB, Han Lee S, Cheol Yoo J. A novel antioxidant peptide, purified from *Bacillus amyloliquefaciens*, showed strong antioxidant potential *via* Nrf-2 mediated heme oxygenase-1 expression. *Food Chem* 2018;**239**:502−10.
15. Jin X, Liu J, Chen YP, Xiang Z, Ding JX, Li YM. Effect of miR-146 targeted HDMCP up-regulation in the pathogenesis of nonalcoholic steatohepatitis. *PLoS One* 2017;**12**:e0174218.
16. Roy S, Benz F, Luedde T, Roderburg C. The role of miRNAs in the regulation of inflammatory processes during hepatofibrogenesis. *Hepatobiliary Surg Nutr* 2015;**4**:24−33.
17. Singh AK, Rooge SB, Varshney A, Vasudevan M, Bhardwaj A, Venugopal SK, et al. Global microRNA expression profiling in the liver biopsies of hepatitis B virus-infected patients suggests specific microRNA signatures for viral persistence and hepatocellular injury. *Hepatology* 2018;**67**:1695−709.
18. Blaya D, Aguilar-Bravo B, Hao F, Casacuberta-Serra S, Coll M, Perea L, et al. Expression of microRNA-155 in inflammatory cells modulates liver injury. *Hepatology* 2018;**68**:691−706.
19. Agarwal V, Bell GW, Nam JW, Bartel DP. Predicting effective microRNA target sites in mammalian mRNAs. *Elife* 2015;**4**:e05005.
20. Böttcher K, Pinzani M. Pathophysiology of liver fibrosis and the methodological barriers to the development of anti-fibrogenic agents. *Adv Drug Deliv Rev* 2017;**121**:3−8.
21. Li W, Zhou C, Fu Y, Chen T, Liu X, Zhang Z, et al. Targeted delivery of hyaluronic acid nanomicelles to hepatic stellate cells in hepatic fibrosis rats. *Acta Pharm Sin B* 2020;**10**:693−710.
22. Zhou J, Huang N, Guo Y, Cui S, Ge C, He Q, et al. Combined obeticholic acid and apoptosis inhibitor treatment alleviates liver fibrosis. *Acta Pharm Sin B* 2019;**9**:526−36.
23. Hernandez-Gea V, Friedman SL. Pathogenesis of liver fibrosis. *Annu Rev Pathol* 2011;**6**:425−56.
24. Mack M. Inflammation and fibrosis. *Matrix Biol* 2018;**68**−**69**:106−21.
25. Bataller R, Brenner DA. Liver fibrosis. *J Clin Invest* 2005;**115**:209−18.
26. Wynn TA, Barron L. Macrophages: master regulators of inflammation and fibrosis. *Semin Liver Dis* 2010;**30**:245−57.
27. Huen SC, Moeckel GW, Cantley LG. Macrophage-specific deletion of transforming growth factor-β1 does not prevent renal fibrosis after severe ischemia−reperfusion or obstructive injury. *Am J Physiol Ren Physiol* 2013;**305**:F477−84.
28. Inagaki Y, Okazaki I. Emerging insights into transforming growth factor beta Smad signal in hepatic fibrogenesis. *Gut* 2007;**56**:284−92.
29. Wang ZL, Deng CY, Zheng H, Xie CF, Wang XH, Luo YF, et al. (*Z*)2-(5-(4-Methoxybenzylidene)-2,4-dioxothiazolidin-3-yl) acetic acid protects rats from CCl_4-induced liver injury. *J Gastroenterol Hepatol* 2012;**27**:966−73.
30. Ong ZY, Wiradharma N, Yang YY. Strategies employed in the design and optimization of synthetic antimicrobial peptide amphiphiles with enhanced therapeutic potentials. *Adv Drug Deliv Rev* 2014;**78**:28−45.
31. Mansour SC, Pena OM, Hancock RE. Host defense peptides: front-line immunomodulators. *Trends Immunol* 2014;**35**:443−50.
32. Zhai Z, Zhang F, Cao R, Ni X, Xin Z, Deng J, et al. Cecropin A alleviates inflammation through modulating the gut microbiota of C57BL/6 mice with DSS-induced IBD. *Front Microbiol* 2019;**10**:1595.
33. Haney EF, Wu BC, Lee K, Hilchie AL, Hancock REW. Aggregation and its influence on the immunomodulatory activity of synthetic innate defense regulator peptides. *Cell Chem Biol* 2017;**24**. 969−980.e4.
34. Liu BH, Jobichen C, Chia CSB, Chan THM, Tang JP, Chung TXY, et al. Targeting cancer addiction for SALL4 by shifting its transcriptome with a pharmacologic peptide. *Proc Natl Acad Sci U S A* 2018;**115**:E7119−28.
35. Mendell JT, Olson EN. MicroRNAs in stress signaling and human disease. *Cell* 2012;**148**:1172−87.
36. Yu F, Lu Z, Chen B, Wu X, Dong P, Zheng J. Salvianolic acid B-induced microRNA-152 inhibits liver fibrosis by attenuating DNMT1-mediated Patched1 methylation. *J Cell Mol Med* 2015;**19**:2617−32.
37. Thounaojam MC, Kundu K, Kaushik DK, Swaroop S, Mahadevan A, Shankar SK, et al. MicroRNA 155 regulates Japanese encephalitis virus-induced inflammatory response by targeting Src homology 2-containing inositol phosphatase 1. *J Virol* 2014;**88**:4798−810.
38. Huffaker TB, O'Connell RM. miR-155−SOCS1 as a functional axis: satisfying the burden of proof. *Immunity* 2015;**43**:3−4.
39. Lan T, Li C, Yang G, Sun Y, Zhuang L, Ou Y, et al. Sphingosine kinase 1 promotes liver fibrosis by preventing miR-19b-3p-mediated inhibition of CCR2. *Hepatology* 2018;**68**:1070−86.
40. Fornes O, Castro-Mondragon JA, Khan A, van der Lee R, Zhang X, Richmond PA, et al. JASPAR 2020: update of the open-access database of transcription factor binding profiles. *Nucleic Acids Res* 2020;**48**:D87−92.
41. Labbé K, Miu J, Yeretssian G, Serghides L, Tam M, Finney CA, et al. Caspase-12 dampens the immune response to malaria independently of the inflammasome by targeting NF-kappaB signaling. *J Immunol* 2010;**185**:5495−502.
42. Saleh M, Mathison JC, Wolinski MK, Bensinger SJ, Fitzgerald P, Droin N, et al. Enhanced bacterial clearance and sepsis resistance in caspase-12-deficient mice. *Nature* 2006;**440**:1064−8.
43. LeBlanc PM, Yeretssian G, Rutherford N, Doiron K, Nadiri A, Zhu L, et al. Caspase-12 modulates NOD signaling and regulates antimicrobial peptide production and mucosal immunity. *Cell Host Microbe* 2008;**3**:146−57.
44. Vande Walle L, Jiménez Fernández D, Demon D, Van Laethem N, van Hauwermeiren F, van Gorp H, et al. Does caspase-12 suppress inflammasome activation?. *Nature* 2016;**534**:E1−4.